



Geophysical Research Letters

RESEARCH LETTER

10.1029/2020GL089519

Key Points:

- This study provides a new perspective on the changes in central Pacific El Niño frequency under global warming
- Models with a stronger cold tongue bias tend to project more frequent central Pacific El Niño
- Emergent constraint indicates that the frequency of CP El Niño in previous projections is overestimated

Supporting Information:

- Supporting Information S1

Correspondence to:

W. Jiang and P. Huang,
huangping@mail.iap.ac.cn;
jiangwenping@hhu.edu.cn

Citation:

Jiang, W., Huang, P., Li, G., & Huang, G. (2020). Emergent constraint on the frequency of central Pacific El Niño under global warming by the equatorial Pacific cold tongue bias in CMIP5/6 models. *Geophysical Research Letters*, 47, e2020GL089519. <https://doi.org/10.1029/2020GL089519>

Received 29 JUN 2020

Accepted 12 SEP 2020

Accepted article online 22 SEP 2020

Emergent Constraint on the Frequency of Central Pacific El Niño Under Global Warming by the Equatorial Pacific Cold Tongue Bias in CMIP5/6 Models

Wenping Jiang^{1,2} , Ping Huang^{2,3,4} , Gen Li¹, and Gang Huang^{2,4} 

¹Key Laboratory of Marine Hazards Forecasting, Ministry of Natural Resources/College of Oceanography/Key Laboratory of Ministry of Education for Coastal Disaster and Protection, Hohai University, Nanjing, China, ²State Key Laboratory of Numerical Modeling for Atmospheric Sciences and Geophysical Fluid Dynamics, Institute of Atmospheric Physics, Chinese Academy of Sciences, Beijing, China, ³Center for Monsoon System Research, Institute of Atmospheric Physics, Chinese Academy of Sciences, Beijing, China, ⁴Laboratory for Regional Oceanography and Numerical Modeling, Qingdao National Laboratory for Marine Science and Technology, Qingdao, China

Abstract El Niño, as the dominant interannual variability for global climate, exhibits different spatial “flavors” with distinct global impacts, and the ensemble of current model projects there will be an increase in the frequency of central Pacific El Niño (CP El Niño) in a warmer world. In this study, we identified that future changes in CP El Niño frequency are significantly related to the simulated cold tongue strength in CMIP5/6 models. A model simulating a stronger cold tongue tends to project more frequent CP El Niño events under global warming, due to the positive zonal advection feedback in the central Pacific. Based on this relationship, we calibrate the CP El Niño frequency projections using the emergent constraint concept and reveal that the changes in CP El Niño frequency under global warming as projected in previous multimodel ensembles more likely decrease because of an excessive cold tongue in CMIP5/6 models.

Plain Language Summary The emerging central Pacific (CP) El Niño has obviously different impacts on global climate compared to the conventional eastern Pacific El Niño. Understanding how CP El Niño will change under global warming is crucial for projecting global climate changes. Previous studies indicated that the CP El Niño frequency will increase under global warming, which ignored the effects of model biases. This study offers a new perspective on the changes in CP El Niño frequency taking into account the effects of the long-standing common bias—the excessive cold tongue—in CMIP5/6 models. We reveal that models with an excessive cold tongue tend to overestimate the changes in ENSO-related SST variability in the CP as well as the CP El Niño frequency in response to global warming.

1. Introduction

As the dominant mode of interannual variability, ENSO exerts significant and far-reaching impacts on global climate and weather (Horel & Wallace, 1981; Ropelewski & Halpert, 1987; Webster et al., 1998). ENSO events are recognized as having two “flavors” with respect to their spatial pattern—one in which the maximum sea surface temperature (SST) anomalies are located in the equatorial eastern Pacific (EP) and the other in the equatorial central Pacific (CP), referred to as EP ENSO and CP ENSO, respectively (Kao & Yu, 2009; Yu & Kim, 2010). The two flavors of ENSO have distinct global climate teleconnections and impacts (Kim et al., 2009; Weng et al., 2009).

In the current situation of increasing anthropogenic greenhouse gas emissions and resultant global warming, understanding how ENSO’s behaviors will change under these conditions is important for projecting the changes in ENSO teleconnections and global extreme events (Cai et al., 2014, 2015; Collins et al., 2010; Latif & Keenlyside, 2009). Coupled general circulation models are most effective tools for projecting ENSO, although the models still have some biases in simulating ENSO characteristics (Bellenger et al., 2014; Cai et al., 2018; Karamperidou et al., 2017; Kim et al., 2014; Kim & Yu, 2012). Previous studies based on the simulations in Phase 3 of the Coupled Model Intercomparison Project (CMIP3) (Yeh et al., 2009) suggested that CP El Niño will occur much more frequently under global warming since the equatorial mean thermocline will rise and flatten in association with weakened Walker circulation and trade winds (Vecchi et al., 2006). In the latest phases of CMIP, that is, CMIP5 and CMIP6, simulations have shown

that the changes in ENSO-related SST (hereafter referred to as “ENSO SST”) variability in 2061–2100 relative to 1961–2000 present a pronounced enhancement in the CP and a significant weakening in the EP (Figure 1a). However, the increased CP El Niño frequency is a matter of debate. On the one hand, it has been found to have increased in the past few decades (Lee & McPhaden, 2010; Liu et al., 2017; Na et al., 2011) but with the observed background changes in the tropical Pacific opposite to the projection in CMIP3 models (McPhaden et al., 2011; Xiang et al., 2013; Yeh et al., 2009). On the other hand, some studies suggested that no consensus has been reached on the changes of CP El Niño frequency in most CMIP5 models (Chen et al., 2017; Power et al., 2013; Taschetto et al., 2014; Xu et al., 2017).

Another uncertainty in the changes of the different ENSO flavors could be the model bias in reproducing the current climatology (Cai et al., 2014; Collins et al., 2010; Huang & Xie, 2015; Taschetto et al., 2014). In several CMIP generations there is a common cold tongue (CT) bias whereby it extends excessively westward into the equatorial western Pacific (Figures 1b and S1 in supporting information) (Li & Xie, 2012, 2014; Zheng et al., 2012). This bias can induce an overly weak cloud radiation-SST feedback in the tropical western Pacific (Feng et al., 2019; Huang & Ying, 2015; Li et al., 2016) and tend to an overestimated trade winds and strong ocean upwelling (Seager et al., 2019), leading to an overly strong SST warming in the tropical western Pacific. The warmer western Pacific mean state facilitates the occurrence of more CP El Niño events (McPhaden et al., 2011; Wang et al., 2019; Xiang et al., 2013) by modifying ENSO’s amplifying and damping feedbacks (Collins et al., 2010; Ham & Kug, 2016; Kim et al., 2014; Latif & Keenlyside, 2009; Zheng et al., 2016). The connection between the background western Pacific state and CP El Niño frequency implies that the CT bias could induce errors in CP El Niño projection by influencing the changes in the background SST pattern, which therefore has the potential to be used as an emergent constraint (Cox et al., 2013, 2018) to correct the projection of changes in CP El Niño. Such an emergent constraint could be applied in model ensembles to reduce the intermodel spread of member projections and correct the multimodel ensemble mean projection—if we can find a significant, physical link between the projected change in CP El Niño and the simulation of an excessive CT bias among the models (Cox et al., 2013, 2018; Huang & Ying, 2015).

In this paper, we examine the effects of the CT bias on projections of CP El Niño frequency under global warming by using 25 CMIP5 models and 14 CMIP6 models. A model with an excessive CT tends to project a larger ENSO SST variability in the CP and more frequent CP El Niño under global warming. With the zonal advection feedback identified as the key process, the emergent constraint concept is utilized to calibrate the projections of CP El Niño frequency, leading to the conclusion that the increase in CP El Niño frequency under global warming is overestimated because of the excessive CT bias.

2. Materials and Methods

2.1. Models and Data

The historical and Representative Concentration Pathway (RCP) 8.5 runs from 25 CMIP5 models (Taylor et al., 2012) and the historical and Shared Socioeconomic Pathway (SSP) 585 runs from 14 CMIP6 models (Eyring et al., 2016) were used in this study. The 25 CMIP5 models were ACCESS1-0, ACCESS1-3, bcc-csm1-1-m, BNU-ESM, CanESM2, CCSM4, CESM1-BGC, CESM1-CAM5, CMCC-CESM, CMCC-CMS, CNRM-CM5, CSIRO-Mk3-6-0, GFDL-ESM 2 M, GFDL-ESM 2G, GISS-E2-H, GISS-E2-R, IPSL-CM5A-LR, IPSL-CM5A-MR, MIROC-ESM, MIROC-ESM-CHEM, MPI-ESM-LR, MPI-ESM-MR, MRI-CGCM3, NorESM1-M, and NorESM1-ME, and the 14 CMIP6 models were BCC-CSM2-MR, CAMS-CSM1-0, CNRM-CM6-1, CNRM-ESM 2-1, CanESM5, EC-Earth3-Veg, FGOALS-f3-L, INM-CM4-8, INM-CM5-0, MCM-UA-1-0, MIROC-ES2L, MIROC6, NESM3, and UKESM1-0-LL.

We used the models’ monthly mean variables, including SST, oceanic potential temperature, zonal current velocity, vertical current velocity, precipitation, and wind. The monthly mean SST data from the Extended Reconstruction of Historical Sea Surface Temperature data set, Version 3 (ERSST3) (Smith et al., 2008), were also used in this study due to the applicability of emergent constraint. All data sets were interpolated to a $2.5^\circ \times 2.5^\circ$ grid.

2.2. Climatology and Change

The historical run from 1961 to 2000 was adopted as a baseline of current climate, while the RCP8.5 run in CMIP5 and SSP585 run in CMIP6 from 2061 to 2100 were employed as future projections under global

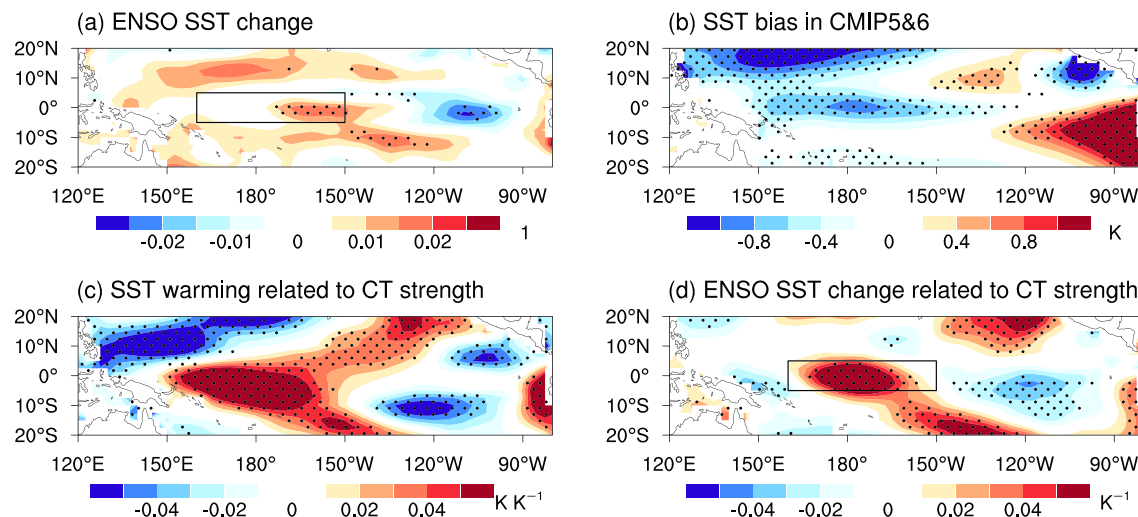


Figure 1. (a) MME changes in ENSO SST in the period 2061–2100 relative to those in 1961–2000. (b) MME climatological SST bias in 39 models relative to observations. (c) Intermodel regression of climatological SST warming onto the CT index. (d) Intermodel regression of ENSO SST change onto the CT index. Stippling in (a) and (b) indicates the regions where the sign of the MME agrees in more than 68% of models. Stippling in (c) and (d) indicates that regressions are significant at the 95% confidence level of the Student's *t* test.

warming. Also, their differences denoted the changes under global warming. All the future changes in each model were normalized by the respective SST change averaged from 60°S to 60°N to remove the influence of intermodel uncertainty with respect to the global mean SST warming.

2.3. Definition of the CT Index

A CT index was defined as the climatological SST averaged over the CT region (2°S to 2°N, 175°E to 90°W) subtracting the tropical Pacific mean SST (30°S to 30°N, 0°–360°E) in the historical run multiplied by −1, to represent CT intensity. The −1 multiplication was used so that a larger CT index value denoted a stronger CT. Figure S1 shows the CT index values in the 25 CMIP5 models and 14 CMIP6 models.

2.4. ENSO SST Variability

Interannual variability signals were obtained by detrending the linear trends of the original data sets and removing the annual cycle and 9-year running mean. Our focus was on boreal winter (December–February, DJF), which is the typical peak season for ENSO. Unless stated otherwise in the text, all results are for the boreal winter season only. The unstandardized Niño-3.4 index (DJF SST anomalies averaged over the region [5°S to 5°N, 120°–170°W]) was regressed onto the anomalies of other variables to denote the ENSO-related variability. The changes in ENSO-related variability in the future were defined as the differences between the regressed ENSO variability in 2061–2100 and 1961–2000. The regression on the unstandardized Niño-3.4 index excluded the effect of ENSO amplitude, with only the structural changes in the ENSO-related variability retained. To remove the effect of the intermodel differences in the global mean SST warming in response to the increasing anthropogenic greenhouse gas among the models, the changes in ENSO-related variables in each model were scaled by their respective mean SST warming averaged from 60°S to 60°N. The multimodel ensemble (MME) was defined simply as the average of the 39 models in CMIP5/6. The intermodel consensus was the percentage of models that agreed on the sign of change with the MME, and a threshold of 68% for the intermodel consensus was equivalent to statistical significance at the 95% confidence level as calculated by the Student's *t* test (Power et al., 2012).

2.5. Selection of CP and EP El Niño Events

EP El Niño events generally show their largest SST anomalies in the Niño-3 region (5°S to 5°N, 90°–150°W), while CP El Niño events tend to peak in the CP within the Niño-4 region (5°S to 5°N, 160°E to 150°W). To classify the spatial structure of different El Niño flavors, we followed the method in Yeh et al. (2009). Specifically, an event was considered as a CP El Niño if the DJF Niño-4 index (SST anomalies averaged over [5°S to 5°N, 160°E to 150°W]) exceeded the DJF Niño-3 index (SST anomalies averaged over [5°S to 5°N, 90°–150°W]).

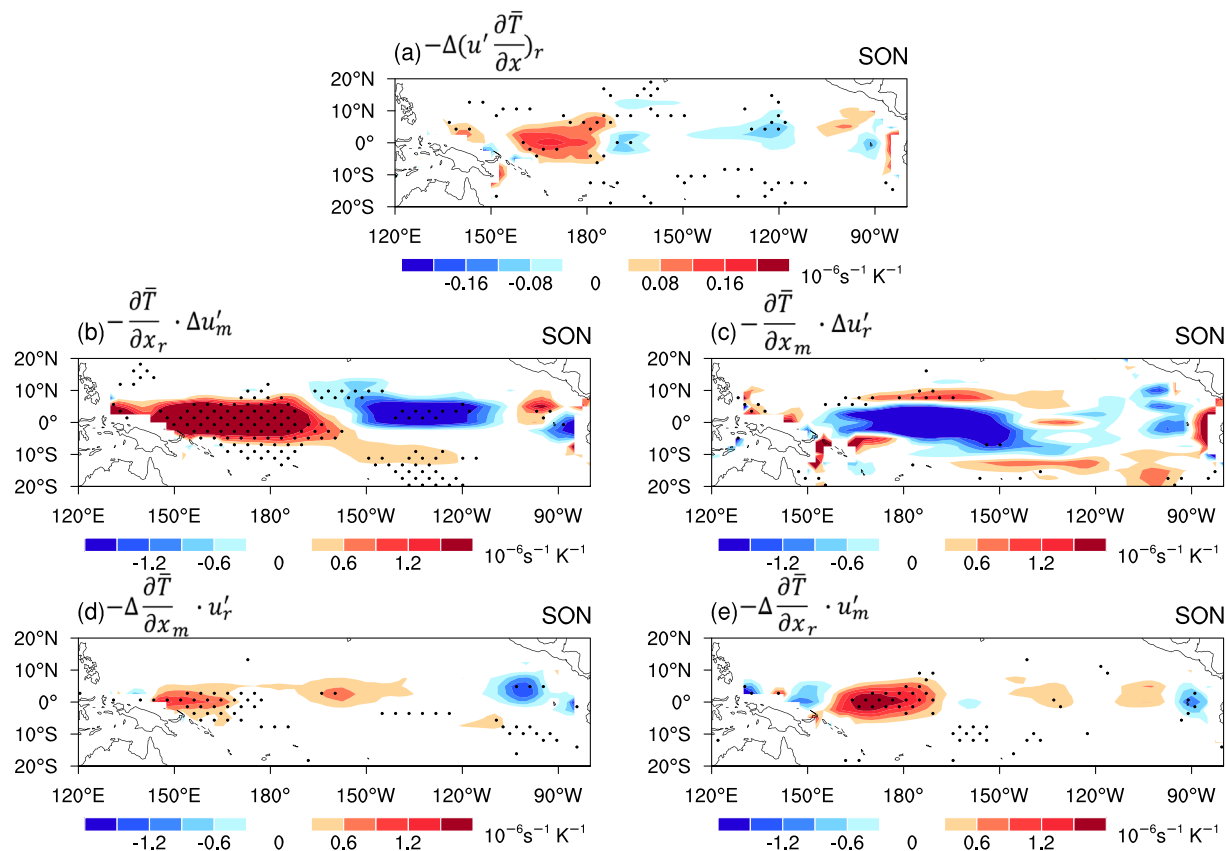


Figure 2. (a) Intermodel regression of changes in zonal advection feedback onto the CT index during the ENSO developing autumn. (b) Intermodel regression of present-day zonal SST gradient multiplied by the MME changes in the ENSO-related zonal current anomaly during the ENSO developing autumn. (c) MME present-day zonal SST gradient multiplied by the intermodel regression of changes in the ENSO-related zonal current anomaly during the ENSO developing autumn. (d) Intermodel regression of the present-day ENSO-related zonal current anomaly multiplied by the MME changes in zonal SST gradient during the ENSO developing autumn. (e) MME present-day ENSO-related zonal current anomaly multiplied by the intermodel regression of changes in zonal SST gradient during the ENSO developing autumn. Stippling in (a)–(e) indicates that regressions are significant at the 95% confidence level.

3. Results

3.1. Relationship Between CT Strength and Changes in ENSO Variability

Figure 1c shows the intermodel regression of the projected changes in the SST mean state onto the CT index. The results display a relationship whereby a model with a stronger simulated CT tends to project a larger SST increase in the equatorial western Pacific and a smaller SST increase in the EP under global warming. In other words, a model with an excessive CT bias tends to project an unrealistic La Niña-like warming, which is consistent with previous studies (Feng et al., 2019; Huang & Ying, 2015; Li et al., 2016). As expected, because of the well-documented connection between the mean state and CP El Niño frequency (McPhaden et al., 2011; Xiang et al., 2013), the changes in ENSO SST variability in the equatorial western-central Pacific around the Niño-4 region are significantly associated with the CT strength among the models (Figure 1d). If we remove several models with the largest CT bias, this relationship is still valid (figures not shown). This result indicates that a model with a stronger CT tends to project a markedly increased SST variability in the Niño-4 region and more frequent CP El Niño in the future.

3.2. Underlying Mechanisms of the Increased CP El Niño Frequency Induced by CT Bias

The development of El Niño is primarily related to three feedbacks: zonal advection feedback; thermocline feedback; and Ekman pumping feedback (Jin et al., 2006; Li, 1997). The zonal advection feedback is defined by the anomalous zonal advection of the mean zonal SST gradient; the thermocline feedback is defined by the mean vertical advection of the anomalous vertical temperature gradient, and the Ekman pumping feedback is defined by the anomalous vertical advection of the mean vertical temperature gradient.

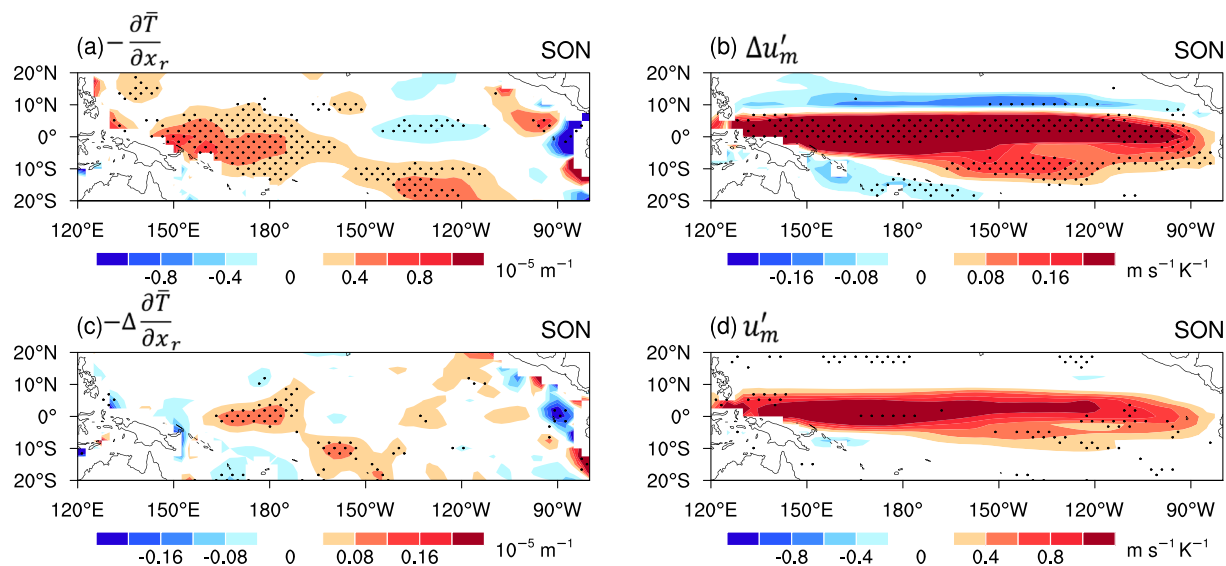


Figure 3. (a) Intermodel regression of the zonal climatological SST gradient in the historical run onto the CT index during the ENSO developing autumn. (b) MME change in the ENSO-related zonal current anomaly during the ENSO developing autumn. (c) Intermodel regression of the change in the zonal climatological SST gradient onto the CT index during the ENSO developing autumn. (d) MME ENSO-related zonal current anomaly in the historical run during the ENSO developing autumn. Stippling in (a) and (c) indicates that regressions are significant at the 95% confidence level. Stippling in (b) and (d) indicates the regions where the sign of the MME agrees in more than 68% of models.

Mathematically, these feedbacks can be expressed as $-u' \frac{\partial \bar{T}}{\partial x} - \bar{w} \frac{\partial T'}{\partial z}$, and $-w' \frac{\partial \bar{T}}{\partial z}$, respectively, where \bar{w} , u' , and w' represent the equatorial mean upwelling, anomalous zonal current, and vertical upwelling, respectively, and \bar{T} and T' denote the anomalous and climatological upper-ocean temperature, respectively. The mixed-layer depth is chosen as a constant of 50 m. Considering that the SST tendency term is orthogonal to the SST anomaly, the budget analysis should be ahead of the SST anomaly several months. Thus, we provided the budget analysis during the ENSO developing autumn (September–November). In the Niño-4 region, the thermocline is thick, and the mean and anomalous vertical temperature gradient are very small in mixed layer. As a result, for the El Niño SST changes in the Niño-4 region, the effects of thermocline feedback and Ekman pumping feedback are negligible (Figure S2), with zonal advection feedback serving as the dominant factor among them (Graham et al., 2017).

The intermodel regression of the projected changes in zonal advection feedback onto the CT index (Figure 2a) displays a zonal dipole pattern in the western-central Pacific, similar to the intermodel regressed SST anomaly changes (Figure 1d). This result implies that zonal advection feedback should be the key process for the increase in CP El Niño related to CT strength. The changes in zonal advection feedback related to different CT strengths can be decomposed into two terms, $-\left(\frac{\partial \bar{T}}{\partial x} \cdot \Delta u'\right)_r$ and $-\left(u' \cdot \Delta \frac{\partial \bar{T}}{\partial x}\right)_r$, where Δ denotes the future change and the subscript r represents the intermodel regression upon the CT index. The terms $-\left(\frac{\partial \bar{T}}{\partial x} \cdot \Delta u'\right)_r$ and $-\left(u' \cdot \Delta \frac{\partial \bar{T}}{\partial x}\right)_r$ are comparable (Figure S3) and can be further decomposed into four terms:

$$-\Delta \left(u' \frac{\partial \bar{T}}{\partial x} \right)_r = -\frac{\partial \bar{T}}{\partial x_r} \cdot \Delta u'_m - \frac{\partial \bar{T}}{\partial x_m} \Delta u'_r - u'_r \cdot \Delta \frac{\partial \bar{T}}{\partial x_m} - u'_m \cdot \Delta \frac{\partial \bar{T}}{\partial x_r},$$

where the subscript m represents the MME. Among the four terms on the right side of the equation, the positive contributions of $-\frac{\partial \bar{T}}{\partial x_m} \Delta u'_r$ and $-u'_r \cdot \Delta \frac{\partial \bar{T}}{\partial x_m}$ to the SST anomaly changes in the CP are negligible (Figures 2b–2e). The $-\frac{\partial \bar{T}}{\partial x_r} \cdot \Delta u'_m$ (Figure 2b) is comparable to $-u'_m \cdot \Delta \frac{\partial \bar{T}}{\partial x_r}$ (Figure 2e), and

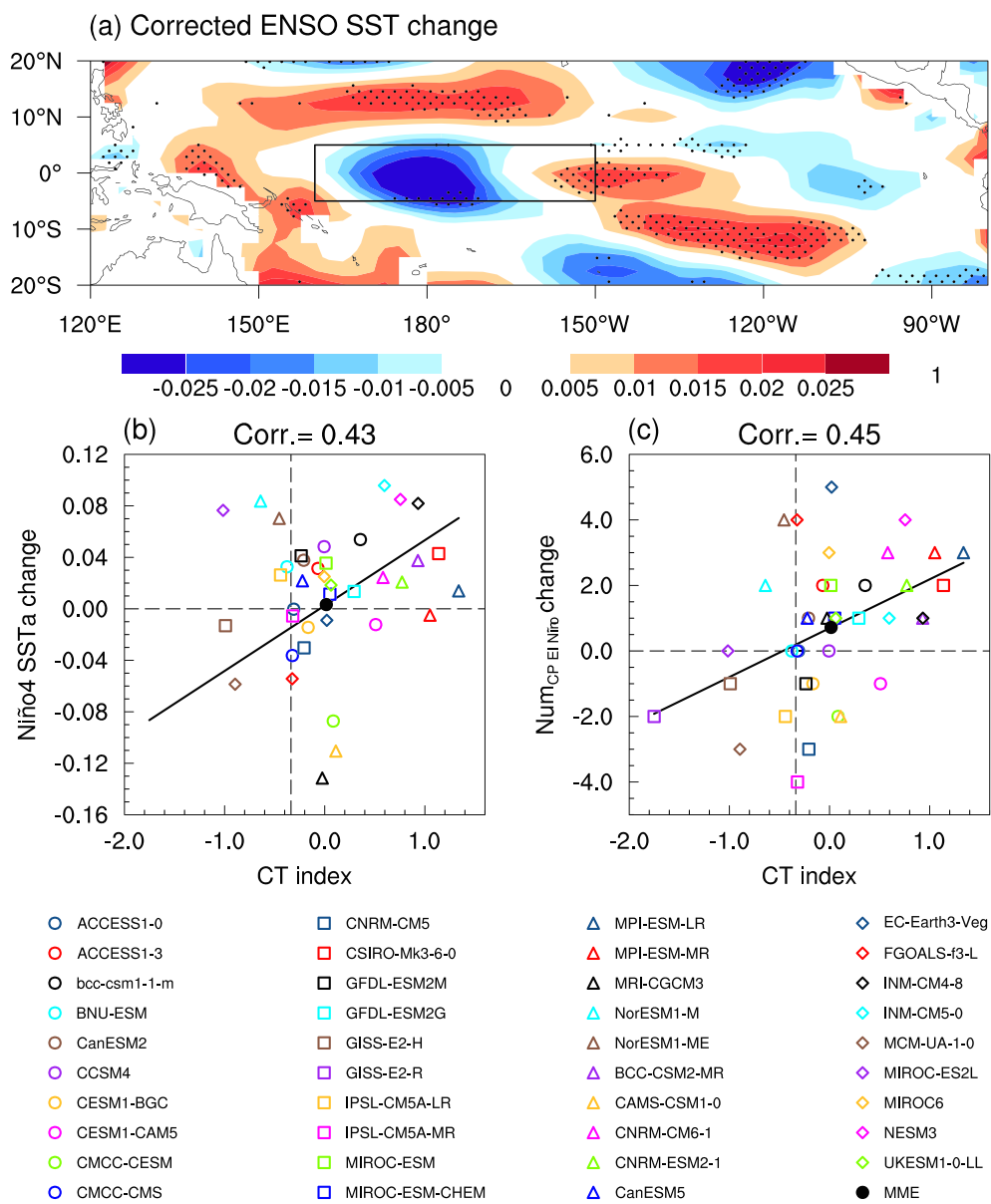


Figure 4. Emergent constraint on ENSO SST variability changes and CP El Niño frequency changes. (a) As in Figure 1c but for corrected MME changes. (b) Scatterplots of the CT index versus projected changes in the Niño-4 SST anomaly. (c) Scatterplots of the CT index versus projected changes in CP El Niño number. The dashed line in the horizontal coordinates denotes the observed present-day CT strength multiplied by -1 . The black solid line denotes the linear fit between the horizontal and vertical coordinates. The intermodel correlation coefficient is shown at the top of panel and is significant at the 99% confidence level, based on the Student's t test. Stippling in (a) indicates that regressions are significant at the 95% confidence level.

their sum largely describes the spatial patterns of zonal advection feedback changes related to CT strength, $-\Delta \left(u' \cdot \frac{\partial \bar{T}}{\partial x} \right)_r$ (Figure 2a).

The spatial patterns of $-\frac{\partial \bar{T}}{\partial x_r} \cdot \Delta u'_m$ (Figure 2b) are dominated by the intermodel spread in the present-day zonal SST gradient related to CT strength ($-\frac{\partial \bar{T}}{\partial x_r}$) shown in Figure 3a, which demonstrates that a model with a cooler CT SST tends to simulate a larger west-minus-east mean zonal SST gradient in the western Pacific, as in previous studies (Graham et al., 2017; Jiang et al., 2017). The ensemble changes in ENSO-related

eastward current anomalies under global warming ($\Delta u'_m$) are likely enhanced (Figure 3b), which might be attributable to the enhancement and eastward shift of El Niño rainfall under global warming (Huang & Xie, 2015; Yan et al., 2020). With the eastward shift in ENSO-related rainfall and convection, the coupled westerly and eastward current anomalies over the equatorial western Pacific both enhance (Figures 3d and S5). The enhanced eastward current anomalies make a positive contribution to zonal advection feedback changes (Figure 2b).

In addition, the spatial pattern of the term $-u'_m \cdot \Delta \frac{\partial \bar{T}}{\partial x_r}$ (Figure 2e) is dominated by the changes in zonal SST gradient related to CT strength ($-\Delta \frac{\partial \bar{T}}{\partial x_r}$) (Figure 3c). A model with a stronger CT tends to project a warmer climatological SST warming in the equatorial western Pacific (Feng et al., 2019; Huang & Ying, 2015; Li et al., 2016), generating a “negative west-positive east” dipole pattern of zonal SST gradient in the western-central Pacific (Figure 3c). Similarly, under the effect of the present-day ENSO-related eastward current anomalies (Figure 3d), a dipole pattern generates in the equatorial western Pacific (Figure 2e), which also contributes to the changes in zonal advection feedback around the Niño-4 region and is favorable for the increased frequency of CP El Niño in the future.

3.3. Emergent Constraint on CP El Niño Frequency Projections

The process of zonal advection feedback gives a reasonable explanation for the connection between current CT strength and future ENSO variability changes among the models. Models with an excessive CT tend to project an increase in ENSO variability in the Niño-4 region (Figure 1d), with a high intermodel correlation of 0.43 exceeding the 99% confidence level (Figure 4b). Thus, we can employ the emergent constraint strategy (Cox et al., 2013, 2018; Huang & Ying, 2015) to correct the increased ENSO variability in the CP in the original MME projection (Figure 1c). Constrained by the observed CT strength, the changes in ENSO SST variability around the Niño-4 region more likely decrease under global warming relative to the original MME projection (Figures 4a and 4b). The effects of the excessive CT on ENSO variability is asymmetric, because that the overly strong SST warming in the tropical western Pacific related to CT strength (Figure 1c) facilitates the occurrence of more CP El Niño events (McPhaden et al., 2011; Xiang et al., 2013). Therefore, the changes in Niño-4 ENSO SST variability related to CT strength mainly come from the changes in CP El Niño frequency related to CT strength. Figure 4c shows that the changes in CP El Niño frequency among the models are also significantly correlated to current CT strength, with a high intermodel correlation of 0.45 exceeding the 99% confidence level. A similar emergent constraint for the changes in Niño-4 ENSO SST variability and CP El Niño frequency indicates that the excessive CT bias exaggerates the increase of Niño-4 ENSO SST variability and CP El Niño frequency under global warming in previous MME projections.

4. Conclusions and Discussion

In this study, we found a significant relationship between the simulated present-day CT strength and the projected changes in Niño-4 ENSO SST variability as well as CP El Niño frequency under global warming in 39 CMIP5/6 models. The stronger the present-day CT, the larger the increase in Niño-4 ENSO SST variability as well as CP El Niño frequency under global warming. When an excessive simulated CT exists, which is common in current state-of-the-art models, the present-day zonal SST gradient and future SST warming in the equatorial western Pacific will be overestimated. These two subsequent situations favor an increase in ENSO SST variability around the Niño-4 region and the occurrence of CP El Niño in a warmer climate. The changes in Niño-4 ENSO SST variability more likely decrease, when constrained by the observed CT strength. This study indicates that improving the simulation of CT strength is important for more reliable projections of ENSO variability and the changes in its different flavors.

It is worth noting that we only found a factor—the excessive CT strength, which can exaggerate the changes in ENSO SST variability in the CP and CP El Niño frequency and explain about 20% of intermodel spread of CP ENSO (El Niño) changes. The changes in Niño-4 ENSO SST variability more likely decrease when constrained by the observed CT strength. If some other factors are found to underestimate the CP El Niño frequency, previous conclusion of increase CP El Niño frequency may be still valid. In addition, the

possible reasons for the enhancement of the ENSO-related zonal current anomalies under global warming, in turn, may be influenced by the change in ENSO SST variability. Further studies may be needed to investigate these open questions.

Data Availability Statement

The ERSST. v3 data are publicly available (at <https://www.esrl.noaa.gov/psd/data/gridded/data.noaa.ersst.html>). The CMIP5 model data sets are available online (at <https://esgf-node.llnl.gov/search/cmip5/>). And the CMIP6 model data sets are publicly available (at <https://esgf-node.llnl.gov/search/cmip6/>).

Acknowledgments

We thank two anonymous reviewers for their constructive comments. This work was supported by the National Natural Science Foundation of China (41831175, 91937302, and 41722504), the Key Deployment Project of Centre for Ocean Mega-Research of Science, Chinese Academy of Sciences (COMS2019Q03), the Fundamental Research Funds for the Central Universities (2018B08314), and the National Key Research and Development Program of China (2019YFA0606703 and 2017YFA0604602).

References

- Bellenger, H., Guilyardi, E., Leloup, J., Lengaigne, M., & Vialard, J. (2014). ENSO representation in climate models: From CMIP3 to CMIP5. *Climate Dynamics*, 42, 1999–2018. <https://doi.org/10.1007/s00382-013-1783-z>
- Cai, W., Borlace, S., Lengaigne, M., van Rensh, P., Collins, M., Vecchi, G., et al. (2014). Increasing frequency of extreme El Niño events due to greenhouse warming. *Nature Climate Change*, 4, 111–116. <https://doi.org/10.1038/nclimate2100>
- Cai, W., Santoso, A., Wang, G., Yeh, S. W., An, S. I., Cobb, K. M., et al. (2015). ENSO and greenhouse warming. *Nature Climate Change*, 5, 849–859. <https://doi.org/10.1038/nclimate2743>
- Cai, W., Wang, G., Dewitte, B., Wu, L., Santoso, A., Takahashi, K., et al. (2018). Increased variability of eastern Pacific El Niño under greenhouse warming. *Nature*, 564(7735), 201–206. <https://doi.org/10.1038/s41586-018-0776-9>
- Chen, C., Cane, M. A., Wittenberg, A. T., & Chen, D. (2017). ENSO in the CMIP5 simulations: Life cycles, diversity, and responses to climate change. *Journal of Climate*, 30, 775–801. <https://doi.org/10.1175/jcli-d-15-0901.1>
- Collins, M., An, S.-I., Cai, W., Ganachaud, A., Guilyardi, E., Jin, F.-F., et al. (2010). The impact of global warming on the tropical Pacific Ocean and El Niño. *Nature Geoscience*, 3(6), 391–397. <https://doi.org/10.1038/ngeo868>
- Cox, P. M., Huntingford, C., & Williamson, M. S. (2018). Emergent constraint on equilibrium climate sensitivity from global temperature variability. *Nature*, 553, 319–322. <https://doi.org/10.1038/nature25450>
- Cox, P. M., Pearson, D., Booth, B. B., Friedlingstein, P., Huntingford, C., Jones, C. D., & Luke, C. M. (2013). Sensitivity of tropical carbon to climate change constrained by carbon dioxide variability. *Nature*, 494, 341–344. <https://doi.org/10.1038/nature11882>
- Eyring, V., Bony, S., Meehl, G. A., Senior, C. A., Stevens, B., Stouffer, R. J., & Taylor, K. E. (2016). Overview of the Coupled Model Intercomparison Project Phase 6 (CMIP6) experimental design and organization. *Geoscientific Model Development*, 9, 1937–1958. <https://doi.org/10.5194/gmd-9-1937-2016>
- Feng, J., Chen, W., Gong, H., Ying, J., & Jiang, W. (2019). An investigation of CMIP5 model biases in simulating the impacts of central Pacific El Niño on the East Asian summer monsoon. *Climate Dynamics*, 52, 2631–2646. <https://doi.org/10.1007/s00382-018-4284-2>
- Graham, F. S., Wittenberg, A. T., Brown, J. N., Marsland, S. J., & Holbrook, N. J. (2017). Understanding the double peaked El Niño in coupled GCMs. *Climate Dynamics*, 48, 2045–2063. <https://doi.org/10.1007/s00382-016-3189-1>
- Ham, Y.-G., & Kug, J.-S. (2016). ENSO amplitude changes due to greenhouse warming in CMIP5: Role of mean tropical precipitation in the twentieth century. *Geophysical Research Letters*, 43, 422–430. <https://doi.org/10.1002/2015GL066864>
- Horel, J. D., & Wallace, J. M. (1981). Planetary-scale atmospheric phenomenon associated with the southern oscillation. *Monthly Weather Review*, 109(4), 813–829. [https://doi.org/10.1175/1520-0493\(1981\)109<0813:PSAPAW>2.0.CO;2](https://doi.org/10.1175/1520-0493(1981)109<0813:PSAPAW>2.0.CO;2)
- Huang, P., & Xie, S.-P. (2015). Mechanisms of change in ENSO-induced tropical Pacific rainfall variability in a warming climate. *Nature Geoscience*, 8, 922–926. <https://doi.org/10.1038/ngeo2571>
- Huang, P., & Ying, J. (2015). A multimodel ensemble pattern regression method to correct the tropical Pacific SST change pattern under global warming. *Journal of Climate*, 28, 4706–4723. <https://doi.org/10.1175/JCLI-D-14-00833.1>
- Jiang, W., Huang, G., Hu, K., Wu, R., Gong, H., Chen, X., & Tao, W. (2017). Diverse relationship between ENSO and the Northwest Pacific summer climate among CMIP5 models: Dependence on the ENSO decay pace. *Journal of Climate*, 30, 109–127. <https://doi.org/10.1175/jcli-d-16-0365.1>
- Jin, F.-F., Kim, S. T., & Bejarano, L. (2006). A coupled-stability index for ENSO. *Geophysical Research Letters*, 33, L23708. <https://doi.org/10.1029/2006GL027221>
- Kao, H.-Y., & Yu, J.-Y. (2009). Contrasting Eastern-Pacific and Central-Pacific types of ENSO. *Journal of Climate*, 22(3), 615–632. <https://doi.org/10.1175/2008jcli2309.1>
- Karamperidou, C., Jin, F.-F., & Conroy, J. L. (2017). The importance of ENSO nonlinearities in tropical pacific response to external forcing. *Climate Dynamics*, 49, 2695–2704. <https://doi.org/10.1007/s00382-016-3475-y>
- Kim, H.-M., Webster, P. J., & Curry, J. A. (2009). Impact of shifting patterns of Pacific Ocean warming on North Atlantic tropical cyclones. *Science*, 325(5936), 77–80. <https://doi.org/10.1126/science.1174062>
- Kim, S. T., Cai, W., Jin, F.-F., & Yu, J.-Y. (2014). ENSO stability in coupled climate models and its association with mean state. *Climate Dynamics*, 42, 3313–3321. <https://doi.org/10.1007/s00382-013-1833-6>
- Kim, S. T., & Yu, J.-Y. (2012). The two types of ENSO in CMIP5 models. *Geophysical Research Letters*, 39, L11704. <https://doi.org/10.1029/2012GL052006>
- Latif, M., & Keenlyside, N. S. (2009). El Niño/Southern Oscillation response to global warming. *Proceedings of the National Academy of Sciences of the United States of America*, 106(49), 20,578–20,583. <https://doi.org/10.1073/pnas.0710860105>
- Lee, T., & McPhaden, M. J. (2010). Increasing intensity of El Niño in the central-equatorial Pacific. *Geophysical Research Letters*, 37, L14603. <https://doi.org/10.1029/2010GL044007>
- Li, G., & Xie, S.-P. (2012). Origins of tropical-wide SST biases in CMIP multi-model ensembles. *Geophysical Research Letters*, 39, L22703. <https://doi.org/10.1029/2012GL053777>
- Li, G., & Xie, S.-P. (2014). Tropical biases in CMIP5 multimodel ensemble: The excessive equatorial Pacific cold tongue and double ITCZ problems. *Journal of Climate*, 27(4), 1765–1780. <https://doi.org/10.1175/jcli-d-13-00337.1>
- Li, G., Xie, S.-P., Du, Y., & Luo, Y. (2016). Effects of excessive equatorial cold tongue bias on the projections of tropical Pacific climate change. Part I: The warming pattern in CMIP5 multi-model ensemble. *Climate Dynamics*, 47, 3817–3831. <https://doi.org/10.1007/s00382-016-3043-5>

- Li, T. M. (1997). Phase transition of the El Niño Southern Oscillation: A stationary SST mode. *Journal of the Atmospheric Sciences*, 54(24), 2872–2887. [https://doi.org/10.1175/1520-0469\(1997\)054<2872:Pten>2.0.CO;2](https://doi.org/10.1175/1520-0469(1997)054<2872:Pten>2.0.CO;2)
- Liu, Y., Cobb, K. M., Song, H., Li, Q., Li, C.-Y., Nakatsuka, T., et al. (2017). Recent enhancement of central Pacific El Niño variability relative to last eight centuries. *Nature Communications*, 8, 15386. <https://doi.org/10.1038/ncomms15386>
- McPhaden, M. J., Lee, T., & McClurg, D. (2011). El Niño and its relationship to changing background conditions in the tropical Pacific Ocean. *Geophysical Research Letters*, 38, L15709. <https://doi.org/10.1029/2011GL048275>
- Na, H., Jang, B.-G., Choi, W.-M., & Kim, K.-Y. (2011). Statistical simulations of the future 50-year statistics of cold-tongue El Niño and warm-pool El Niño. *Asia-Pacific Journal of Atmospheric Sciences*, 47(3), 223–233. <https://doi.org/10.1007/s13143-011-0011-1>
- Power, S., Delage, F., Chung, C., Kociuba, G., & Keay, K. (2013). Robust twenty-first-century projections of El Niño and related precipitation variability. *Nature*, 502, 541–545. <https://doi.org/10.1038/nature12580>
- Power, S. B., Delage, F., Colman, R., & Moise, A. (2012). Consensus on twenty-first-century rainfall projections in climate models more widespread than previously thought. *Journal of Climate*, 25(11), 3792–3809. <https://doi.org/10.1175/jcli-d-11-00354.1>
- Ropelewski, C. F., & Halpert, M. S. (1987). Global and regional scale precipitation associated with the El Niño/Southern Oscillation. *Monthly Weather Review*, 115(8), 1606–1626. [https://doi.org/10.1175/1520-0493\(1987\)115<1606:garspp>2.0.co;2](https://doi.org/10.1175/1520-0493(1987)115<1606:garspp>2.0.co;2)
- Seager, R., Cane, M., Henderson, N., Lee, D.-E., Abernathay, R., & Zhang, H. (2019). Strengthening tropical Pacific zonal sea surface temperature gradient consistent with rising greenhouse gases. *Nature Climate Change*, 9(7), 517–522. <https://doi.org/10.1038/s41558-019-0505-x>
- Smith, T. M., Reynolds, R. W., Peterson, T. C., & Lawrimore, J. (2008). Improvements to NOAA's historical merged land-ocean surface temperature analysis (1880–2006). *Journal of Climate*, 21(10), 2283–2296. <https://doi.org/10.1175/2007jcli2100.1>
- Taschetto, A. S., Sen Gupta, A., Jourdain, N. C., Santoso, A., Ummenhofer, C. C., & England, M. H. (2014). Cold tongue and warm pool ENSO events in CMIP5: Mean state and future projections. *Journal of Climate*, 27, 2861–2885. <https://doi.org/10.1175/jcli-d-13-00437.1>
- Taylor, K. E., Stouffer, R. J., & Meehl, G. A. (2012). An overview of CMIP5 and the experiment design. *Bulletin of the American Meteorological Society*, 93(4), 485–498. <https://doi.org/10.1175/bams-d-11-00094.1>
- Vecchi, G., Soden, B. J., Wittenberg, A., Held, I. M., Leetmaa, A., & Harrison, M. (2006). Weakening of tropical Pacific atmospheric circulation due to anthropogenic forcing. *Nature*, 441(7089), 73–76. <https://doi.org/10.1038/nature04744>
- Wang, B., Luo, X., Yang, Y.-M., Sun, W., Cane, M. A., Cai, W., et al. (2019). Historical change of El Niño properties sheds light on future changes of extreme El Niño. *Proceedings of the National Academy of Sciences of the United States of America*, 116, 22,512–22,517. <https://doi.org/10.1073/pnas.1911130116>
- Webster, P. J., Magana, V. O., Palmer, T. N., Shukla, J., Tomas, R. A., Yanai, M., & Yasunari, T. (1998). Monsoons: Processes, predictability, and the prospects for prediction. *Journal of Geophysical Research*, 103(C7), 14,451–14,510. <https://doi.org/10.1029/97JC02719>
- Weng, H., Behera, S. K., & Yamagata, T. (2009). Anomalous winter climate conditions in the Pacific rim during recent El Niño Modoki and El Niño events. *Climate Dynamics*, 32(5), 663–674. <https://doi.org/10.1007/s00382-008-0394-6>
- Xiang, B., Wang, B., & Li, T. (2013). A new paradigm for the predominance of standing central Pacific warming after the late 1990s. *Climate Dynamics*, 41, 327–340. <https://doi.org/10.1007/s00382-012-1427-8>
- Xu, K., Tam, C.-Y., Zhu, C., Liu, B., & Wang, W. (2017). CMIP5 projections of two types of El Niño and their related tropical precipitation in the twenty-first century. *Journal of Climate*, 30, 849–864. <https://doi.org/10.1175/jcli-d-16-0413.1>
- Yan, Z., Wu, B., Li, T., Collins, M., Clark, R., Zhou, T., et al. (2020). Eastward shift and extension of ENSO-induced tropical precipitation anomalies under global warming. *Science Advances*, 6, eaax4177. <https://doi.org/10.1126/sciadv.aax4177>
- Yeh, S.-W., Kug, J.-S., Dewitte, B., Kwon, M.-H., Kirtman, B. P., & Jin, F.-F. (2009). El Niño in a changing climate. *Nature*, 461(7263), 511–514. <https://doi.org/10.1038/nature08316>
- Yu, J. Y., & Kim, S. T. (2010). Three evolution patterns of Central-Pacific El Niño. *Geophysical Research Letters*, 37, L08706. <https://doi.org/10.1029/2010GL042810>
- Zheng, X.-T., Xie, S.-P., Lv, L.-H., & Zhou, Z.-Q. (2016). Intermodel uncertainty in ENSO amplitude change tied to Pacific ocean warming pattern. *Journal of Climate*, 29, 7265–7279. <https://doi.org/10.1175/jcli-d-16-0039.1>
- Zheng, Y., Lin, J.-L., & Shinoda, T. (2012). The equatorial Pacific cold tongue simulated by IPCC AR4 coupled GCMs: Upper ocean heat budget and feedback analysis. *Journal of Geophysical Research*, 117, C05024. <https://doi.org/10.1029/2011JC007746>